Hadronic light-by-light scattering in the muon $g-2$: A Dyson-Schwinger equation approach

Tobias Goecke,[1] Christian S. Fischer,[2,3] and Richard Williams[1]

[1]*Institute for Nuclear Physics, Darmstadt University of Technology, Schlossgartenstraße 9, 64289 Darmstadt, Germany*
[2]*Institut für Theoretische Physik, Universität Giessen, 35392 Giessen, Germany*
[3]*Gesellschaft für Schwerionenforschung mbH, Planckstr. 1 D-64291 Darmstadt, Germany*

(Received 7 January 2011; published 4 May 2011)

We determine the hadronic light-by-light scattering contribution to the anomalous magnetic moment of the muon using the framework of Dyson-Schwinger and Bethe-Salpeter equations of QCD. Our result for the pseudoscalar (π^0, η, η') meson-exchange diagram is commensurate with previous calculations. In our calculation of the quark-loop contribution we improve upon previous approaches by explicitly implementing constraints due to gauge invariance. The impact of transverse contributions, presumably dominated by vector-meson poles, are only estimated at this stage. As a consequence, our value $a_\mu^{\mathrm{LBL;quarkloop}} = (136 \pm 59) \times 10^{-11}$ is significantly larger. Taken at face value, this then leads to a revised estimate of the total $a_\mu = 116\,591\,891.0(105.0) \times 10^{-11}$.

DOI: 10.1103/PhysRevD.83.094006 PACS numbers: 12.38.Lg, 13.40.Em, 13.40.Gp, 14.60.Ef

I. INTRODUCTION

One of the most impressive successes of the standard model (SM) of particle physics is the determination of the anomalous magnetic moment of the electron. This quantity is determined both experimentally and theoretically to such a degree of precision that the underlying physical description is vindicated. However, when it comes to the question of new physics, the anomalous magnetic moment of the muon is an even more interesting quantity, see e.g. [1–3] for reviews. This is due to the large mass of the muon as compared to the electron, which leads to an enhanced sensitivity to physics in and beyond the standard model. Experimental efforts at Brookhaven and theoretical efforts of the past ten years have pinned a_μ down to the 10^{-11} level, leading to significant deviations between theory [1] and experiment [4]:

$$\text{Experiment}: 116\,592\,089.0(63.0) \times 10^{-11}, \quad (1)$$

$$\text{Theory}: 116\,591\,790.0(64.6) \times 10^{-11}. \quad (2)$$

While the theoretical and experimental values are determined to comparable errors, the central values give rise to a discrepancy at the 3.3σ confidence level. This difference has been present for a number of years and can be interpreted as a signal for the existence of physics beyond the standard model. However, to clearly distinguish between new physics and possible shortcomings in the SM calculations the uncertainties present in both experimental and theoretical values of a_μ need to be further reduced.

The greatest uncertainties in the theoretical determination of a_μ are encountered in the hadronic contributions, i.e., those terms which involve QCD beyond perturbation theory. The most prominent of these is given by the vacuum polarization tensor dressing of the QED vertex, see Fig. 1(a). Fortunately it can be related to experimental data of e^+e^- annihilation and τ decay via dispersion relations and the optical theorem, thus resulting in a precise determination with systematically improvable errors [1]. Considered individually, its (leading and subleading order) contribution to the anomalous magnetic moment of the muon is [2]

$$[6\,903.0(52.6) - 100.3(1.1)] \times 10^{-11}. \quad (3)$$

Although currently these uncertainties dominate the error of the theoretical result in Eq. (2) it is foreseeable that future experiments reduce this error below that of another, more problematic source. This is the hadronic light-by-light (LBL) scattering diagram, shown in Fig. 1(b). This contribution cannot be directly related to experiment and must hence be calculated entirely through theory. The central object in such a calculation is the photon four-point function. It receives important contributions from the small momentum region below 2 GeV, where perturbative QCD breaks down and nonperturbative methods are imperative. Recent determinations of a_μ^{LBL} are provided in Table I. Although the magnitude of the LBL contribution is much

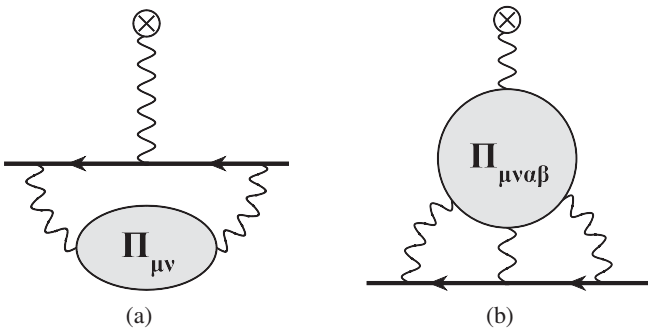

FIG. 1. The two classifications of corrections to the photon-muon vertex function are shown: (a) hadronic vacuum polarization contribution to a_μ. The vertex is dressed by the vacuum polarization tensor $\Pi_{\mu\nu}$; (b) the hadronic light-by-light scattering contribution to a_μ.

TABLE I. Recent calculations of the hadronic light-by-light scattering contribution to the anomalous magnetic moment of the muon are shown.

Reference	a_μ^{LBL}
[5]	$116(40) \times 10^{-11}$
[6]	$105(26) \times 10^{-11}$
[7]	$110(40) \times 10^{-11}$
[8–10]	$89(15) \times 10^{-11}$

smaller than the one from vacuum polarization it is significant because its error is of a comparable size. Taken together, with the errors added in quadrature, the hadronic contributions constitute the largest uncertainty in the standard model determination of the anomalous magnetic moment of the muon.

The theoretical approaches to determine the LBL contribution are centered around two main ideas. One is chiral symmetry, its breaking pattern and the associated low energy effective descriptions of QCD [11]; the other is the large-N_c expansion of the four-photon function and the associated ordering of diagrams. These ideas have been put together in [12] and led to various refined calculations of LBL within the frameworks of large-N_c and vector-meson dominance [5,13–15], the extended Nambu-Jona-Lasinio model (ENJL) [7,16], the (very similar) hidden local symmetry model [8–10], or a nonlocal chiral quark model [17,18], see also [6] for a summary. Although in terms of diagrams individual contribution are of varying size in these approaches, their sum leads to consistent results as can be inferred from Table I. In all these calculations the [pseudoscalar (PS)] meson exchange contributes the most and the meson loop has been found to be small. A possible explanation of the latter is given in [14]. As a result, we quote the recent value for LBL $a_\mu^{\mathrm{LBL}} = 105(26) \times 10^{-11}$ proposed in Ref. [6], which also agrees with the one in [5].

One of the most important goals for these and future calculations is the reduction of the model dependence and subsequently of the systematic error involved in these calculations. Since LBL is nonperturbative in nature, all estimates in Table I are plagued by systematic model dependencies. It is therefore desirable to also explore other calculational tools which have the potential to go beyond these limitations. Certainly, lattice gauge theory is one such method. However, due to the multiscale nature of the problem no reliable estimates for LBL have been extracted on the lattice so far. This multiscale nature also makes EFT methods less desirable as it proves more difficult to impose suitable matching conditions.

Another nonperturbative method, well suited to accommodate for largely different scales, is the framework of Dyson-Schwinger and Bethe-Salpeter equations [19–22]. In the past years this approach has been used to study fundamental properties of QCD such as confinement and dynamical chiral symmetry breaking. On the other hand the approach served as a tool for hadron physics. In this work we expand upon this and apply the formalism to a calculation of the LBL contribution to the muon anomalous magnetic moment. To this end we separate different contributions to the light-by-light four-point function according to their topology of gluon exchange and their status with respect to the large-N_c expansion. Diagrammatically this translates to considering resummations of planar diagrams involving gluon exchange. In this scheme we then determine the dressed quark-loop diagram and an approximation in terms of pseudoscalar meson (π^0, η, η') exchange contributions. In principle, the off-shell meson amplitudes involved in these diagrams could be calculated from inhomogeneous Bethe-Salpeter equations. Here, due to numerical complexity, in this work we resort to a commonly used ansatz that extrapolates on-shell wave functions. Our results are then compared with the ones of previous approaches. First results of our analysis have been published in Ref. [23]. Here we discuss our method in much more detail and present new and more elaborate results for the quark-loop diagram.

The paper is organized thus: in Sec. II we recall the definition of the light-by-light scattering amplitude and focus upon the pseudoscalar-pole contributions; in Sec. III we introduce our Dyson-Schwinger approach and discuss the necessary truncation schemes; in Sec. IV we present and discuss our results. We conclude in Sec. V.

II. THE LBL SCATTERING AMPLITUDE

In the hadronic light-by-light scattering contribution, Fig. 1(b), the muon is coupled to an external photon source via the hadronic photon four-point function $\Pi_{\mu\nu\alpha\beta}$, defined through

$$\Pi_{\mu\nu\alpha\beta}(q_1, q_2, q_3) = \int_{xyz} e^{iq_1\cdot x + iq_2\cdot y + iq_3\cdot z} \langle j_\mu(0) j_\nu(x) j_\alpha(y) j_\beta(z)\rangle, \quad (4)$$

where $\int_{xyz} = \int d^4x \int d^4y \int d^4z$ represents integration over four-dimensional space, $q_{1,2,3}$ are the photon momenta that are connected to the muon line, and j_μ is the electromagnetic quark current

$$j_\mu = \tfrac{2}{3}\bar{u}\gamma_\mu u - \tfrac{1}{3}\bar{d}\gamma_\mu d - \tfrac{1}{3}\bar{s}\gamma_\mu s + \tfrac{2}{3}\bar{c}\gamma_\mu c. \quad (5)$$

A detailed discussion of this object can be found in the literature, see, e.g., [14,16]. Instead of working directly with the light-by-light scattering diagram given in Fig. 1(b), it is more convenient to follow the strategy employed in Refs. [24,25]. Here gauge symmetry is exploited to construct quantities that are finite. Through use of the Ward-Takahashi-identity $k_\mu \Pi_{\mu\nu\alpha\beta} = 0$ it follows via differentiation that

$$\Pi_{\rho\nu\alpha\beta} = -k_\mu \frac{\partial}{\partial k_\rho} \Pi_{\mu\nu\alpha\beta} =: -k_\mu \tilde{\Pi}_{(\rho)\mu\nu\alpha\beta}, \quad (6)$$

which serves as definition of the five-point-function $\tilde{\Pi}_{(\rho)\mu\nu\alpha\beta}$. Here $k = q_1 + q_2 + q_3$ is the momentum of the external photon. The virtue of the derivative is that it lowers the dimensionality of the integral thus ensuring that integrals employing $\tilde{\Pi}_{(\rho)\mu\nu\alpha\beta}$ are manifestly convergent. We define the quantity

$$ie\tilde{\Gamma}_{\rho\mu} = \int_{q_1}\int_{q_2} D_{\epsilon\nu}(q_1) D_{\delta\alpha}(q_2) D_{\gamma\beta}(q_3) \times (ie\gamma_\gamma) S(p_1) \times (ie\gamma_\delta) S(p_2) (ie\gamma_\epsilon) \times [(ie)^4 \tilde{\Pi}_{(\rho)\mu\nu\alpha\beta}(q_1, q_2, q_3)], \quad (7)$$

which is now related to the dressed muon vertex Γ_μ of Fig. 1(b) via

$$ie\Gamma_\mu = iek_\rho \tilde{\Gamma}_{\rho\mu}. \quad (8)$$

Here $D_{\mu\nu}(q)$ are perturbative photon propagators (we use Feynman gauge) with momenta q_i. The perturbative muon propagators are given by $S(p)$.

The anomalous magnetic moment can now be obtained by applying the appropriate projection operator to Eq. (7)

$$a_\mu = \frac{1}{48 m_\mu} \mathrm{tr}[(i\not{P} + m_\mu)[\gamma_\sigma, \gamma_\rho](i\not{P} + m_\mu)\tilde{\Gamma}_{\sigma\rho}]|_{k\equiv 0}, \quad (9)$$

that we write here in Euclidean convention for later convenience. Using Eqs. (6)–(9) we are able to evaluate the light-by-light scattering contributions for an arbitrary photon four-point function. What remains now is the specification of this four-point function within our approach.

A. Expansion using EFT approaches

As already mentioned in the Introduction, chiral and large-N_c arguments have been established to expand the full LBL scattering amplitude into the diagrammatic parts shown in Fig. 2 [1]. These diagrams belong to different orders with respect to chiral and large-N_c counting. Whereas the meson-exchange diagrams and the quark-loop diagram are leading in large-N_c, it is the meson-loop diagram that is leading in the chiral counting. Thus, *a priori*, one does not know which expansion is to be preferred. Therefore it is certainly interesting that all explicit calculations of these contributions seem to favor the N_c-counting scheme; meson-loop contributions have been found to be suppressed. Arguments as to why this is the case have been presented in Ref. [14].

Strictly speaking, however, one does not actually perform a large-N_c expansion as this would necessitate the inclusion of an infinite number of resonances. Instead, only the lowest lying meson-exchange contributions in the pseudoscalar, scalar and axial-vector channel have been subsummed. Here, the pseudoscalar π^0 exchange has been identified as the leading contribution, followed by η and η' exchange.

Concerning the PS exchange contribution a few remarks are in place. The photons in the exchange diagrams are coupled to the PS mesons via the PS-$\gamma\gamma$ form factor, $F_{\mathrm{PS}\gamma\gamma}$. It is evident that there are two limiting features of the pseudoscalar-pole approximation. The first is the actual provision of the form factors themselves, which are in general subject to systematic errors depending on how they are modeled or calculated. The second is the procedure under which the form factor is taken off-shell. Previous approaches mainly used vector-meson dominance ideas to determine this form factor and there has been an extensive debate as to whether and how short distance constraints have to be implemented [5,6,13,14,18]. Rather than employ the principles of vector-meson dominance and construct an ansatz for the on-shell/off-shell form factor, we wish to calculate it from first principles. This is possible within the framework of Dyson-Schwinger and Bethe-Salpeter equations using a well explored and successful truncation scheme [20].

As for the quark-loop diagram, different interpretations have been given in the literature. Whereas in [12] it has been argued that the quark loop is a separate contribution that has to be added to the other two, in many other approaches it has been treated as a complementary one, which is only added in the large spacelike momentum region, say above a typical cutoff for an effective model. In our functional approach, described below, it is clearly the first point of view that is correct. Moreover, as we will see, the quark loop is subject to large dressing effects not only for the quark propagators in the loop but also for the quark-photon vertices. This will be the main result of our work.

B. Expansion using functional methods

From a functional integral approach to QCD, featuring quarks and gluons as the fundamental degrees of freedom, the analogous picture to what is normally considered in the literature is shown in Fig. 3, where we give an expansion in terms of nonperturbatively dressed one-particle irreducible Green's functions. The basic idea of this expansion is not a separation of long distance and short distance scales, but rather a separation of different classes of diagrams based on their topology. Clearly, the expansion is such that no double counting of diagrams is involved. By considering a restricted subset of contributions in which only diagrams with a planar topology are resummed, we effectively adhere to the N_c-counting scheme as favored in the EFT approaches mentioned above. Though there are similarities between the two pictures, since we work with a truncated formulation of exact-QCD rather than an effective field theory there are some differences that we will comment on here to avoid confusion. First of all, our quarks are to be interpreted in the same way as those extracted via Lattice

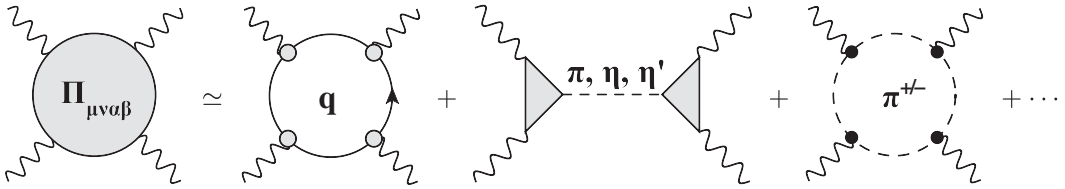

FIG. 2. The hadronic LBL scattering contribution to a_μ and its expansion, using EFT approaches, as a quark-loop part (left), leading pseudoscalar meson-exchange part (middle), and a leading meson-loop part (right), is shown. Note that the quarks here may be interpreted differently to those in Fig. 3.

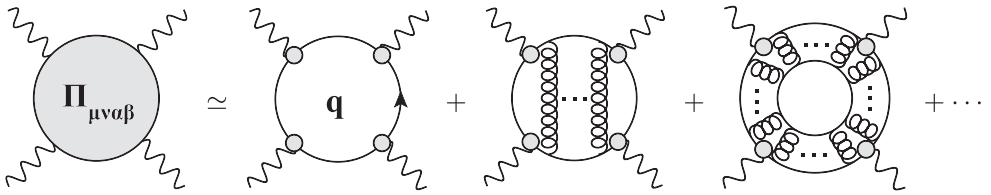

FIG. 3. The hadronic LBL scattering contribution to a_μ and its expansion, using functional methods, as a quark-loop part (left), a ladder-exchange part (middle), and a ladder-ring part (right), is shown. All propagators and vertices are fully dressed, with the ellipsis marks indicating that an infinite number of gluons are resummed.

QCD; they are characterized by momentum dependent dressing functions that interpolate between the current and constituent quark limits, cf. the discussion below Fig. 11. Second, the quark-photon coupling is a nonperturbative form factor and not merely a tree-level bare vertex; it can be calculated self-consistently for a given truncation scheme. Finally, the planar resummation of gluons is related to the T matrix of quark-antiquark scattering and contains meson poles that can be associated with pseudoscalars, vectors, scalars etc. This will be exploited below, where we return to the conventional meson-exchange picture to approximate these contributions.

We wish to emphasize that the expansion displayed in Fig. 3 has been used successfully in a different context already in Ref. [26]. There π-π scattering has been considered using similar quark-box and ladder-exchange parts as displayed in Fig. 3. In this setup, the authors of Ref. [26] could reproduce the isospin 0 and 2 scattering lengths in exact agreement with Weinberg's low energy results. Moreover, in Ref. [27] it has been checked, that the corresponding resonant expansion similar to the one displayed in Fig. 2 is a good approximation to the ladder-exchange part of Fig. 3. Note that in both these calculations the quark-box diagram had to be added to the ladder-exchange or the resonant ''meson-exchange'' part, respectively. We believe that these results add further support to our approach.

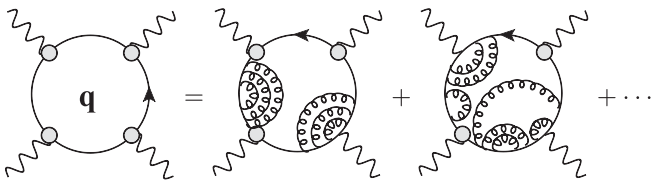

FIG. 4. The expansion of quark-loop contribution to the photon four-point function in terms of planar quark and gluon diagrams (all propagators are fully dressed) is shown.

1. Quark-loop contribution

Within our proposed truncation, the quark-loop is composed of dressed quark propagators and dressed quark-photon vertices. On expanding these one-particle irreducible Green's functions, within the rainbow-ladder approximation, we find planar-like diagrams such as the ones shown in Fig. 4 (all propagators are fully dressed), where in fact infinite ladders of gluons are taken into account. Should we consider corrections beyond rainbow ladder, such as those considered in Refs. [28,29], one would also include diagrams in which the gluons have self-interactions as well as crossed-ladder components. Taking into account such corrections is, however, beyond the scope of the present work.

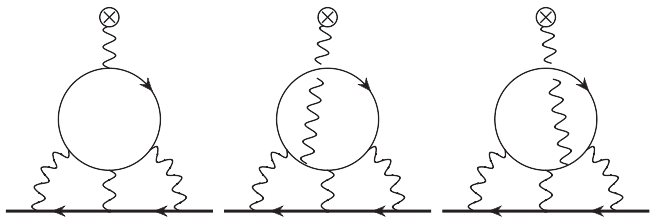

FIG. 5. The hadronic light-by-light scattering contributions to a_μ from the quark loop are shown. There are an additional three diagrams (not shown) in which the quark-spin line is reversed. Principally, these diagrams involve dressed quark propagators and quark-photon vertices.

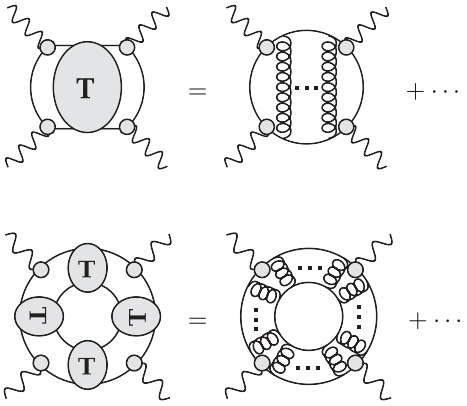

FIG. 6. The ladder-exchange contribution (upper equation) and ring-ladder contribution (lower equation) to the photon four-point amplitude are shown.

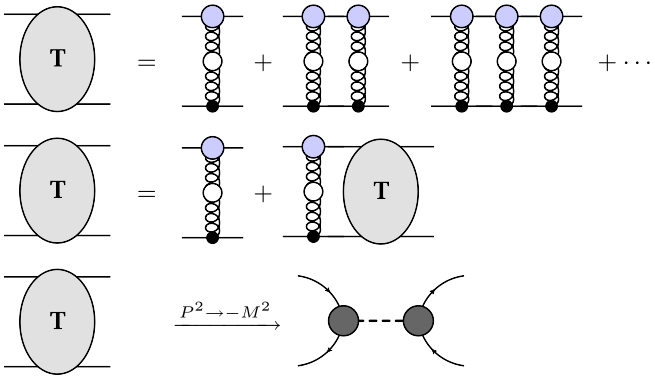

FIG. 7 (color online). The T matrix in the rainbow-ladder approximation is shown. The top diagram shows the series expansion in terms of dressed quarks and gluon, while the middle represents Dyson's equation. The bottom diagram shows the pole ansatz for the T matrix on-mass-shell.

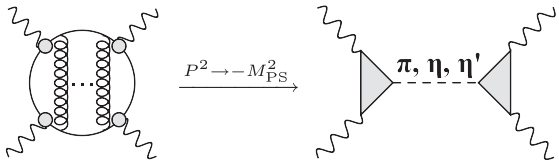

FIG. 8. The pole representation of the ladder-exchange contribution to the photon four-point function is shown.

Considering this contribution to the muon-photon vertex, we obtain the diagrams as shown in Fig. 5, where we have shown permutation of the external photon legs but have omitted the topologies that merely involve reversal of the quark-spin line (these give identical contributions and hence constitute a factor of 2). As is well known, these diagrams are individually logarithmically divergent with only their sum finite and convergent; thus one employs the aforementioned trick, Eq. (6), of taking the derivative of the photon four-point function [24,25].

Since this is now to be applied to loop integrals over nonperturbative quantities, namely, the quark propagator, it is no longer possible to reduce the integration to be five-dimensional as in the case of perturbative studies. More generally, on considering the planar nature of the diagrams, one must deal with 8-dimensional integrals which necessitate Monte Carlo methods [30]. However, for reasons of calculational simplicity we actually integrate in nine. We did check, however, that we were able to reproduce the well-known perturbative results for the electron loop contribution to the anomalous magnetic of the electron and the muon [31–33]. Additionally, due to the somewhat involved Dirac algebra [34,35] we will content ourselves with taking the quark-photon vertices inside the quark-loop contribution to be: (a) bare, (b) 1BC, (c) full BC. The precise meaning of these abbreviations and the relation to the full quark-photon vertices will become clear in Secs. III B and IV B. The extension to employ the numerically calculated nonperturbative form of the vertex will be explored in a later publication. The results of our calculation are presented in Sec. IV.

2. Ladder-exchange and ladder-ring contribution

Two contributions that are leading and subleading in large N_c respectively are the so-called ladder-exchange and ladder-ring diagrams of Fig. 3. These infinite ladder resummations are in fact related to the T matrix of bound-state theory in a certain approximation scheme (that produces planar diagrams). Thus, another way to portray these contributions is given in Fig. 6.

The T matrix in rainbow-ladder approximation is given in Fig. 7. At this point, we make it clear that there is no conflict nor double counting between the quark-loop and ladder-exchange diagrams, as they clearly consider and resum different topologies of diagrams.

As it stands, the full T matrix is a very complicated object to solve in its entirety though its structure admits several approximations and simplifications [36]. The one which we employ here is similar to the viewpoint taken by effective field theory approaches; that is, we consider pole contributions to be dominant. Now, since it is well-known that such an *infinite* gluon-ladder resummation dynamically generates bound-state poles, one can expand the T matrix in terms of meson pole contributions as shown in Fig. 7 (bottom diagram). On mass shell we then have a unique definition of the Bethe-Salpeter amplitude, described below in Sec. III A, that gives the form factor describing coupling of a meson to two quarks. From this point the (on-shell) pseudoscalar-photon-photon form factor can be defined and calculated, giving rise to the "leading" pseudoscalar meson-exchange part, as shown in Fig. 8 and Fig. 9. In a similar fashion, the ring-ladder diagram contains contributions akin to the pion loop on meson mass shell. However, since these are generally considered to be subleading we will not consider them further here and instead concentrate on the quark-loop and ladder-exchange

FIG. 9 (color online). The Dyson-Schwinger equation for the quark-propagator is shown. Specification of the fully dressed gluon propagator (wiggly line) and quark-gluon vertex (shaded blob) defines the truncation scheme.

diagrams. After we present our approach and formalism in the next section, results will be discussed in Sec. IV.

III. FRAMEWORK

The dressed quark propagator is one of the most important quantities in the covariant description of mesons. It encodes nonperturbative properties of QCD such as dynamical mass generation and the realization of a nonzero condensate. Its equation of motion, the quark Dyson-Schwinger equation (DSE) displayed in Fig. 10, also contains the dressed gluon propagator and a dressed quark-gluon vertex. Whereas the dressed gluon propagator in Landau gauge is a well-known quantity by now, see [37–40] and references therein,[1] the study of the details of the dressed quark-gluon vertex is still on an exploratory level, although some progress has been made in the past years [29,42,43]. Pending deeper insights into the nonperturbative structure of the quark-gluon interaction it is therefore reasonable to work with approximations that take into account important features of the full theory. This strategy, of course, introduces model dependencies into our calculation that have to be carefully addressed later on.

From a phenomenological perspective a successful approximation in this respect is the rainbow-ladder truncation of the quark DSE. The philosophy here is to combine the dressing of the gluon propagator with the vector part of the quark-gluon vertex into a single function depending on the gluon momentum only. While this is certainly a severe approximation in principle, in practice it turned out to be very successful concerning the calculation of masses and electromagnetic properties of mesonic observables [20]. While the parameters of the model are tuned such that it reproduces the experimental values for the masses and decay constants of the pion, it also reproduces the pion charge radius and $\pi\gamma\gamma$ transition form factors on the percent level. In the vector channel the agreement with experimental masses and decay constants is on the five and 10% level. Thus, while one has to keep in mind possible systematic caveats, we nevertheless believe that such a model is an excellent starting point for a systematic evaluation of hadronic LBL.

[1]There is an intense debate on the behavior of the gluon propagator in the deep infrared, i.e., for momenta $p \leq 50$ MeV. It seems, however, that this momentum region is irrelevant when it comes to the calculation of observables [28,29,41].

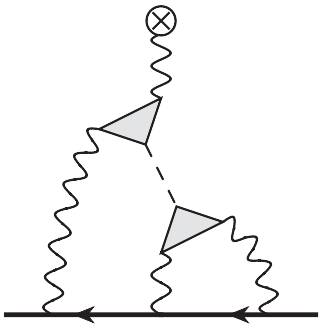

FIG. 10. The pion-pole part of the LBL contribution to a_μ is shown. The three possible permutations of the photon legs are not shown.

In Euclidean momentum space, the renormalized dressed gluon and quark propagators in the Landau gauge are given by

$$D_{\mu\nu}(p) = \left(\delta_{\mu\nu} - \frac{p_\mu p_\nu}{p^2}\right)\frac{Z(p^2;\mu^2)}{p^2}, \tag{10}$$

$$S_F(p) = \frac{Z_f(p^2;\mu^2)}{i\not{p} + M(p^2)} = \frac{1}{i\not{p}A(p^2;\mu^2) + B(p^2;\mu^2)}, \tag{11}$$

where $Z(p^2;\mu^2)$ is the gluon dressing function, $Z_f(p^2;\mu^2)$ is the quark wave function, and $M(p^2)$ is the renormalization point independent quark mass function. The dependence of such functions on the renormalization point μ^2 will be implicitly assumed from here on. The quark dressing functions $A(p^2)$ and $B(p^2)$ can be recombined into the quark mass and wave function by $M(p^2) = B(p^2)/A(p^2)$ and $Z_f(p^2) = 1/A(p^2)$.

These propagators may be obtained by solving their respective Dyson-Schwinger equations. The DSE for the quark propagator, shown diagrammatically in Fig. 10, is written

$$S^{-1}(p) = Z_2 S_0^{-1}(p) + \Sigma(p),$$
$$\Sigma(p) = g^2 C_F Z_{1F} \int \frac{d^4q}{(2\pi)^4}\Gamma_\nu(q,p) D_{\mu\nu}(k)\gamma_\mu S_F(q), \tag{12}$$

where $\Sigma(p)$ is the quark self-energy, $k = p - q$ and the Casimir $C_F = 4/3$ stems from the color trace. We introduced the reduced quark-gluon vertex $\Gamma_\nu(q, p)$ defined by $\Gamma^a_\nu(q, p) = ig\frac{\lambda^a}{2}\Gamma_\nu(q, p)$. The bare inverse quark propagator is $S_0^{-1}(p) = i\not{p} + m$. The renormalization factors are $Z_{1F} = Z_2/\tilde{Z}_3$ for the quark-gluon vertex, Z_2 for the quark-propagator, and $\tilde{Z}_3$ for the ghost dressing function.

The scalar dressing functions of the quark DSE are solved for by appropriate projections of Eq. (12). This is a coupled nonlinear integral equation that is solvable provided we know the gluon dressing function and the structure of the quark-gluon vertex. In the rainbow approximation both are specified by Ansätze, with, in particular, the choice $\Gamma_\nu(q, p) := \Gamma^{\mathrm{YM}}(k^2)\gamma_\nu$, with scalar

function $\Gamma^{\rm YM}$ representing the nonperturbative dressing of the quark-gluon vertex and $k = q - p$ the gluon momenta. Here, the gluon dressing function $Z(k^2)$ from Eq. (10) and the Yang-Mills part $\Gamma^{\rm YM}(k^2)$ of the quark-gluon vertex are combined to form a phenomenological effective interaction. For the Maris-Tandy (MT) model [44] this function is given by

$$Z(k^2)\Gamma^{\rm YM}(k^2) = \frac{4\pi}{g^2}\left(\frac{\pi}{\omega^6} D k^4 \exp(-k^2/\omega^2) + \frac{2\pi\gamma_m}{\log(\tau + (1 + k^2/\Lambda_{\rm QCD}^2)^2)} \times [1 - \exp(-k^2/[4m_t^2])]\right), \quad (13)$$

with

$$m_t = 0.5 \text{ GeV}, \qquad \tau = e^2 - 1$$
$$\gamma_m = 12/(33 - 2N_f), \qquad \Lambda_{\rm QCD} = 0.234 \text{ GeV}.$$

This interaction corresponds to a Gaussian distribution in the infrared that provides for sufficient interaction strength to generate dynamical chiral symmetry breaking , together with the one-loop behavior of the running coupling at large, perturbative, momenta. The latter is mandatory to provide for the correct short distance behavior of the quark propagator. The remaining parameters ω and D essentially constitute a single one-parameter family of solutions for which pion observables remain comparable, via $\omega D = (0.72 \text{ GeV})^3$.

For the convenience of the reader, in Fig. 11 we again show the two dressing functions $Z_f(p^2)$ and $M(p^2)$ that characterize the nonperturbative quark propagator,

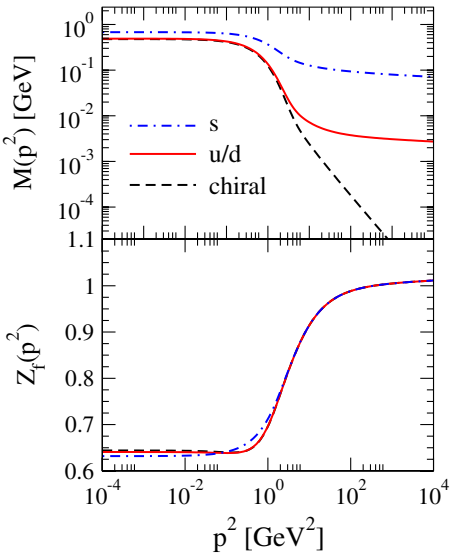

FIG. 11 (color online). Mass function and wave-function dressing functions corresponding to quark propagators solved with the Maris-Tandy interaction [44] are shown.

obtained by solving Eq. (12) using the Maris-Tandy interaction [44]. Clearly, in the mass function there are three distinguished momentum regions. In the infrared, the quark propagator is essentially constant displaying the behavior of a constituent quark. Then for 1 GeV$^2 < p^2 <$ 10 GeV^2 there is a region of rapid change, where the quark mass function follows the well-known $1/p^2$ behavior expected from the operator product expansion. For even larger momenta and nonvanishing current quark mass, the quark mass function behaves logarithmically as expected for a current quark. The fully dressed quark propagator thus naturally interpolates between the constituent and current quark picture. We consider this feature of the Dyson-Schwinger approach to QCD as an advantage compared with effective models such as the ENJL model.

A. Bethe-Salpeter equation

The chiral symmetry preserving truncation for the Bethe-Salpeter equation, consistent with the rainbow approximation above, is given by the ladder approximation

$$\Gamma^{q\bar{q}}_{tu}(p;P) = \int \frac{d^4k}{(2\pi)^4} K_{tu;rs}(p,k;P) \times [S_F(k_+)\Gamma^{q\bar{q}}(k;P)S_F(k_-)]_{sr} \quad (14)$$

with the kernel $K_{tu;rs}$ given by

$$K_{tu;sr}(q,p;P) = \frac{g^2 Z(k^2)\Gamma^{\rm YM}(k^2)Z_{1F}}{k^2}\left(\delta_{\mu\nu} - \frac{k_\mu k_\nu}{k^2}\right) \times \left[\frac{\lambda^a}{2}\gamma_\mu\right]_{ts}\left[\frac{\lambda^a}{2}\gamma_\nu\right]_{ru}, \quad (15)$$

see Fig. 12 for a graphical representation. Here $\Gamma^{q\bar{q}}(p;P)$ is the Bethe-Salpeter vertex function corresponding to a pseudoscalar quark antiquark bound state, specified below. The momenta $k_+ = k + P/2$ and $k_- = k - P/2$ are such that the total momentum P of the meson is given by $P = k_+ - k_-$ and the relative momentum $k = (k_+ + k_-)/2$. The Latin indices (t, u, r, s) of the kernels refer to color, flavor, and Dirac structure.

The form of the kernel Eq. (15) is uniquely determined from the axial-vector Ward-Takahashi identity and ensures that the pion is a Goldstone boson in the chiral limit without any fine-tuning of parameters. It also ensures that important constraints from chiral symmetry such as the Gell-Mann-Oakes-Renner relation are satisfied.

In general, the covariant structure of the Bethe-Salpeter vertex function, $\Gamma^{q\bar{q}}(p;P)$, determines the quantum numbers of the bound state under consideration. In particular, a pseudoscalar meson is completely specified by the following form:

$$\Gamma^{q\bar{q}}(p;P) = \gamma_5[F_1^{q\bar{q}}(p;P) - i\not{P}F_2^{q\bar{q}}(p;P) - i\not{p}(p\cdot P)F_3^{q\bar{q}}(p;P) - [P,p]F_4^{q\bar{q}}(p;P)]. \quad (16)$$

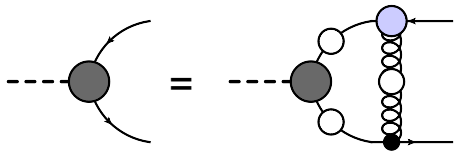

FIG. 12 (color online). The homogeneous Bethe-Salpeter equation for the meson amplitude is shown.

This amplitude is obtained through the solution of Eq. (14) on-mass shell: $P^2 = -m_{q\bar{q}}^2$ in Euclidean space. While (16) represents a quark antiquark bound state, physical mesons are defined as matrices in flavor space built out of the $q\bar{q}$ amplitudes. This then leads to the same decomposition as in Eq. (16) but with flavor-matrix valued quantities Γ and F_i. In the following, however, we will keep the flavor index implicit and use Eq. (16) for $q\bar{q}$ amplitudes and mesons alike. Anyway, in the isospin-limit considered herein the pion amplitude differs from the $u\bar{u}/d\bar{d}$ amplitudes only by flavor-matrix structure. The pole masses and the scalar amplitudes that contain the dynamical information are identical (up to normalization). This is different for the η and η'.

In the chiral limit the leading behavior of the pion amplitude $\hat{\Gamma}^\pi$ is given by

$$\hat{F}_1^\pi(p;P) := \lambda_3 B(p^2)/f_\pi, \tag{17}$$

where $B(p^2)$ is the scalar dressing function of the quark, f_π is the chiral limit value of the leptonic decay constant, and λ_3 is a Gell-Mann matrix that represents the flavor structure. The hat in Eq. (17) indicates that the object is matrix valued in flavor space. The expressions for the calculation of f_π and the normalization condition of the Bethe-Salpeter amplitude together with details on the numerical procedure for dealing with the Bethe-Salpeter equation are given in [45]. For the convenience of the reader we display the resulting Bethe-Salpeter amplitudes for $p^2 = -m_\pi^2$ and $p.P = 0$ in Fig. 13. Qualitatively, the amplitudes have a similar form as the quark mass function in the chiral limit. For large momenta and up to logarithmic corrections

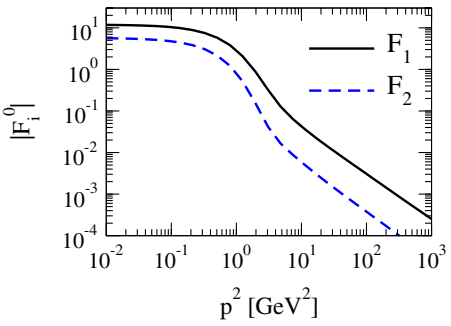

FIG. 13 (color online). Normalized Bethe-Salpeter amplitudes F_1 and F_2 of the pion solved with the Maris-Tandy interaction (leading Chebyshev component) [44] are shown.

they fall off like $1/p^2$, which is a necessary condition to correctly describe the anomalous decay of the pion and to reproduce the asymptotics of the pion form factor [46].

B. Quark-photon vertex

An important quantity for the determination of the LBL contribution to the muon $g-2$ is the dressed quark-photon vertex. This quantity is genuinely nonperturbative in nature and necessary for the calculation of the PS$\gamma\gamma$ form factor. It describes the coupling of a fully dressed quark to a photon and is dominated by QCD corrections. As a function of one Lorentz and two spinor indices, it can be decomposed into 12 Dirac structures

$$\Gamma_\mu(P,k) = \sum_{i=1}^{12} \lambda_i(P,k) V_\mu^i(P,k), \tag{18}$$

where $V_\mu^i(P,k)$ represents the basis components, and $\lambda_i(P,k)$ the nonperturbative dressing functions. A common basis is that of Ball and Chiu [47], in which $V_\mu^i(P,k)$ is split into terms that are transverse and nontransverse with respect to the photon momentum. The Ward-Takahashi identity and regularity assumptions constrain the form of the nontransverse part in terms of quark-propagator functions

$$\begin{aligned}\Gamma_\mu^{\mathrm{BC}}(k,P) := \Bigg[& \gamma_\mu \frac{A(k_+^2)+A(k_-^2)}{2} \\ & + (\not{k}_+ + \not{k}_-)(k_+ + k_-)_\mu \frac{1}{2}\frac{A(k_+^2)-A(k_-^2)}{k_+^2-k_-^2} \\ & + i(k_+ + k_-)_\mu \frac{B(k_+^2)-B(k_-^2)}{k_-^2-k_+^2}\Bigg],\end{aligned} \tag{19}$$

leaving only the strictly transverse pieces undetermined. Equation (19) can therefore be seen as an approximation of the full vertex and has been used in situations where the full vertex cannot be determined numerically.

A more sophisticated approach, however, is to solve the inhomogeneous Bethe-Salpeter equation of the quark-photon vertex, shown diagrammatically in Fig. 14. It is given by

$$\Gamma_{tu}^\mu(k,P) = Z_1 \gamma_{tu}^\mu + \int_q K_{tu;rs}[S_F(k_+)\Gamma^\mu(q,P)S_F(k_-)]_{sr}, \tag{20}$$

where Z_1 is the renormalization factor associated with the quark-photon vertex. By using the same interaction kernel as in the Bethe-Salpeter equation for mesons, Eq. (15), not only do we achieve self-consistency within the truncation scheme, but also by virtue of its symmetry preserving nature we satisfy the Ward-Takahashi identity. Consequently, the nontransverse part of the vertex, given in Eq. (19), is nicely reproduced numerically, with transverse terms additionally generated [48–51].

We note here that such a determination of the quark-photon vertex automatically contains poles in the timelike

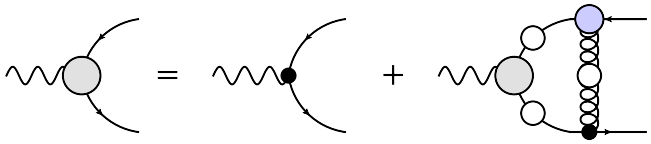

FIG. 14 (color online). The inhomogeneous BS equation for the quark-photon vertex, in rainbow-ladder approximation, is shown.

region corresponding to vector meson exchange. Thus, presupposing that vector-meson dominance is an important feature in the structure of the pion electromagnetic form factor, it is already included here as a result of the approach we employ. This has been discussed in detail also in Refs. [48,49].

The numerical details involved in the calculation of the quark-photon vertex have been described in several works, see, e.g., the appendix of Ref. [51]. Below we will use the fully dynamical, self-consistent solution of Eq. (20) for our calculation of the PS $\to \gamma\gamma$ form factor and the resulting meson-exchange contribution to LBL. Unfortunately, because of the numerical complexity we have to restrict ourselves to the exact longitudinal part given by Eq. (19) in the quark-loop diagram. It will be a subject of future work to overcome this limitation.

C. The PS $\to \gamma\gamma$ form factor

The coupling of the exchanged pseudoscalar mesons to photons is the quantity that is central to the resonant expansion of Fig. 2. In impulse approximation, consistent with the rainbow-ladder truncation scheme introduced in Sec. III, the Bethe-Salpeter amplitude is connected via a quark triangle to the fully dressed quark-photon vertex, as shown in Fig. 15. For a pseudoscalar PS we have

$$\Lambda^{\mathrm{PS}\gamma^*\gamma^*}_{\mu\nu}(k_1,k_2) = 2e^2N_c\int_k \mathrm{tr}[i\hat{\mathcal{Q}}_e\Gamma_\nu(k_2,p_{12})S_F(p_2) \times \hat{\Gamma}^{\mathrm{PS}}(p_{23},P)S_F(p_3)i\hat{\mathcal{Q}}_e\Gamma_\mu(k_1,p_{31})S_F(p_3)], \quad (21)$$

where k_1 and k_2 are the outgoing photon momenta; $p_1 = q$, $p_2 = q - k_2$, and $p_3 = q + k_1$ are the quark momenta; and $p_{ij} = (p_i + p_j)/2$. The factor of 2 stems from an exchange of the two photon vertices and $\hat{\mathcal{Q}} = \mathrm{diag}[2/3, -1/3, -1/3]$ gives the quark's charge. The PS vertex $\hat{\Gamma}^{\mathrm{PS}}$ is explicitly matrix valued in flavor space. It is defined as

$$\pi^0\colon \hat{\Gamma}^{\pi^0} = \frac{1}{\sqrt{2}}\mathrm{diag}[\Gamma^{u\bar{u}}, -\Gamma^{d\bar{d}}, 0],$$
$$\eta^8\colon \hat{\Gamma}^{\eta^8} = \frac{1}{\sqrt{6}}\mathrm{diag}[\Gamma^{u\bar{u}}, \Gamma^{d\bar{d}}, -2\Gamma^{s\bar{s}}],$$
$$\eta^0\colon \hat{\Gamma}^{\eta^0} = \frac{1}{\sqrt{3}}\mathrm{diag}[\Gamma^{u\bar{u}}, \Gamma^{d\bar{d}}, \Gamma^{s\bar{s}}], \quad (22)$$

for the pseudoscalar mesons. The $\Gamma^{q\bar{q}}$ are solutions of Eq. (14). In addition we work in the isospin-limit ($\Gamma^{u\bar{u}} = \Gamma^{d\bar{d}}$). Since the quantities in Eq. (22) are defined in the singlet-octet basis we have to rotate in order to obtain the η-η' amplitudes

$$\hat{\Gamma}^{\eta} = \cos\theta\hat{\Gamma}^{\eta^8} - \sin\theta\hat{\Gamma}^{\eta^0},$$
$$\hat{\Gamma}^{\eta'} = \sin\theta\hat{\Gamma}^{\eta^8} + \cos\theta\hat{\Gamma}^{\eta^0}, \quad (23)$$

where we haven taken $\theta = -15.4°$ [52]. The pseudoscalar electromagnetic form factor can be described by a single scalar function, $F^{\pi\gamma^*\gamma^*}$. For the pion this function can be given a natural normalization via the Abelian anomaly [53]

$$\Lambda^{\pi\gamma^*\gamma^*}_{\mu\nu}(k_1^2,k_2^2) = i\frac{\alpha_{\mathrm{em}}}{\pi f_\pi}\varepsilon_{\mu\nu\alpha\beta}k_1^\alpha k_2^\beta F^{\pi\gamma^*\gamma^*}(k_1^2,k_2^2), \quad (24)$$

where α_{em} is the fine structure constant and f_π the pion decay constant. The definition of the prefactors is such that $F^{\pi\gamma\gamma}(0,0) = 1$. The η and η' mesons have the same tensor structure.

Note that the form factors determined here do not accurately reflect all effects due to the topological mass of the η_0, simply because the $U_A(1)$ anomaly is not represented correctly in the Maris-Tandy model.[2] In the form factors this may be a minor problem. The effect is larger, however, in the meson propagators attached to the form factors. We therefore prefer to use the experimental masses in these propagators, thereby taking care of the majority of the $U_A(1)$-anomaly effects.

The π^0 electromagnetic form factor has been explored in detail in Ref. [50], wherein it has been confirmed that the correct normalization is satisfied. In addition it has been shown analytically (and numerically) that the correct asymptotic behavior, modulo potential logarithms, is obtained [50,57]

$$\lim_{Q^2\to\infty} F^{\pi^0\gamma\gamma^*}(0,Q^2) \propto \frac{1}{Q^2}\lim_{Q^2\to\infty} F^{\pi^0\gamma^*\gamma^*}(Q^2,Q^2) \propto \frac{1}{Q^2}. \quad (25)$$

In Fig. 16 we plot the form factor as a function of the two photon momenta k_1^2 and k_2^2 and compare with the vector-meson dominance (VMD) inspired model used in Ref. [13]. One clearly sees that both form factors agree nicely on a qualitative and even quantitative level. Whereas the low-momentum behavior is governed by the anomaly, at large momenta both form factors fall off according to Eqs. (25). There are small quantitative differences in the

[2]Perspectives to improve this issue in the framework of Dyson-Schwinger equations have been reported in Refs. [54–56]. In Ref. [56] a topological mass of the η_0 has been obtained which goes well with lattice results of the topological susceptibility via the Witten-Veneziano relation.

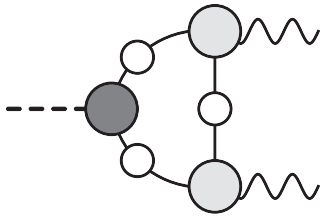

FIG. 15. The $\pi^0\gamma\gamma$ form factor in impulse approximation is shown. All internal quantities are fully dressed.

midmomentum regime, which will lead to a small difference in the meson-exchange contributions to LBL, discussed below. In general, however, the results of our calculation may be viewed as a confirmation of the previously used model approaches almost from first principles.

D. Off-shell prescription

It is evident from the kinematics of the diagram shown in Fig. 9 that the form factors, thus far defined as on-shell quantities, must be evaluated for momenta of the exchanged pseudoscalar meson that would be far from the pole mass. In the approach considered here, the pseudoscalar amplitude is obtained from its homogeneous Bethe-Salpeter equation and hence is by definition an on-shell quantity. Thus, to proceed we must introduce a prescription for the continuation of this quantity to the off-shell momentum region.

Since the off-shell behavior should be dominated by the pseudoscalar-pole contribution, the introduction of any prescription that provides for a suppression at off-shell momentum should be a suitable starting point. Here, we will employ a prescription that is inspired from the axial-vector Ward-Takahashi identity in the chiral limit

$$2P_\mu \Gamma^{5,3}_\mu(k,P) = iS^{-1}(k_+)\gamma_5 + i\gamma_5 S^{-1}(k_-). \tag{26}$$

Here the axial-vector vertex is defined as the correlation function $\Gamma^{5,3}_\mu = \langle j^{5,3}_\mu q\bar{q}\rangle$ that includes the axial-vector current in the pion channel $j^{5,3}_\mu = \bar{q}\gamma_\mu\gamma^5\frac{\lambda^3}{2}q$. It is clear that Eq. (26) relates $\Gamma^{5,3}_\mu$ to the quark propagator. Taking explicit parametrizations for vertex and propagator (see [45]) that include the pion pole in the axial-vector vertex, the following form of the dominant amplitude for the π^0 can be deduced:

$$\hat{F}^{\pi}_1(k,P) = \lambda_3 \frac{B(k_+) + B(k_-)}{2f_\pi}. \tag{27}$$

Here $k_\pm = k \pm P/2$. Note that in the chiral on-shell limit ($P^2 = 0$) the above equation reduces to Eq. (17). We

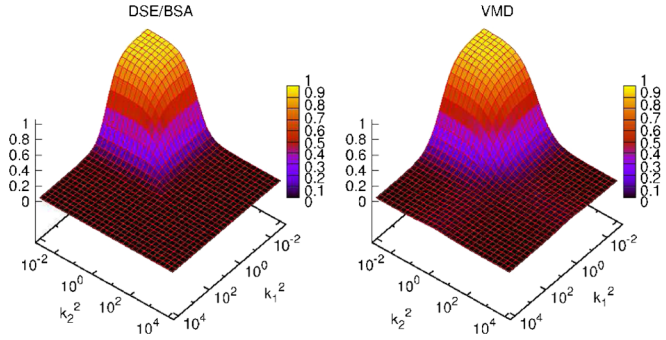

FIG. 16 (color online). The $\pi \to \gamma\gamma$ form factor plotted as a function of the two photon momenta k_1^2 and k_2^2 is shown. We compare our numerical results in the Dyson-Schwinger/Bethe-Salpeter approach with an ansatz inspired by vector-meson dominance discussed in Ref. [5].

generalize the pseudoscalar amplitude, Eq. (16), by using Eq. (27) as a guideline for all four structures also away from the chiral limit. The final off-shell meson amplitude reads

$$\begin{aligned}\hat{\Gamma}^{\rm PS} = \gamma_5[&\hat{F}^{\rm PS}_1(p;P) + f(P^2)\{-i\not{P}\hat{F}^{\rm PS}_2(p;P) \\ &- i\not{p}(p\cdot P)\hat{F}^{\rm PS}_3(p;P) - [\not{P},\not{p}]\hat{F}^{\rm PS}_4(p;P)\}],\end{aligned} \tag{28}$$

where the hat over the functions $\hat{F}^{\rm PS}_i$ indicates that the flavor structure of the corresponding meson is included in the same manner as in Eqs. (22) and (23). The scalar off-shell amplitudes $F^{q\bar{q}}_i(k,P)$ are defined in terms of the on-shell amplitudes[3] $F^{q\bar{q}}_i(k, k\cdot P)$ through

$$F^{q\bar{q}}_i(k,P) = \frac{F^{q\bar{q}}_i(k_+, k_+\cdot P) + F^{q\bar{q}}_i(k_-, k_-\cdot P)}{2}, \tag{29}$$

for which $i = 1,\ldots,4$. The on-shell amplitudes are obtained via Eq. (14). In order to account for the mass dimensions of the form factors $\hat{F}^{\rm PS}_{2,3,4}$ we attach to each the function

$$f(P^2) = \sqrt{\frac{m^2_{\rm PS}}{P^2 + 2m^2_{\rm PS}}}. \tag{30}$$

This prevents an unnatural enhancement at high meson virtuality while at the same time leaving the on-shell behavior unchanged. The off-shell form factor

$$\Lambda^{{\rm PS}^*\gamma^*\gamma^*}_{\mu\nu}(P,k_1,k_2) = \epsilon_{\mu\nu\alpha\beta}k_1^\alpha k_2^\beta \mathcal{F}_{{\rm PS}^*\gamma^*\gamma^*}(P^2,k_1^2,k_2^2), \tag{31}$$

is then obtained via the generalization of Eq. (21) by taking the Bethe-Salpeter amplitude $\Gamma^{q\bar{q}}$ to be defined via Eq. (28).

The contribution to the derivative of the four-point-function can now be written as [13]

[3]With a slight abuse of notation we denote off-shell quantities to depend on P whereas on-shell they depend only on $k\cdot P$ with $P^2 = -m^2_{\rm PS}$.

$$\tilde{\Pi}_{(\rho)\mu\nu\lambda\sigma}(q_1, q_2, -q_{12}) = \frac{\mathcal{F}_{\mathrm{PS}^*\gamma^*\gamma^*}(q_{12}^2, q_1^2, q_2^2)\mathcal{F}_{\mathrm{PS}^*\gamma^*\gamma^*}(q_{12}^2, q_{12}^2, 0)}{q_{12}^2 + m_{\mathrm{PS}}^2} \epsilon_{\mu\nu\alpha\beta} q_1^\alpha q_2^\beta \epsilon_{\lambda\sigma\rho\tau} q_{12}^\tau + \frac{\mathcal{F}_{\mathrm{PS}^*\gamma^*\gamma^*}(q_1^2, q_1^2, 0)\mathcal{F}_{\mathrm{PS}^*\gamma^*\gamma^*}(q_1^2, q_2^2, q_{12}^2)}{q_1^2 + m_{\mathrm{PS}}^2} \epsilon_{\mu\sigma\tau\rho} q_1^\tau \epsilon_{\nu\lambda\alpha\beta} q_1^\alpha q_2^\beta + \frac{\mathcal{F}_{\mathrm{PS}^*\gamma^*\gamma^*}(q_2^2, q_1^2, q_{12}^2)\mathcal{F}_{\mathrm{PS}^*\gamma^*\gamma^*}(q_2^2, q_2^2, 0)}{q_2^2 + m_{\mathrm{PS}}^2} \epsilon_{\mu\lambda\alpha\beta} q_1^\alpha q_2^\beta \epsilon_{\nu\sigma\rho\tau} q_2^\tau, \quad (32)$$

where $q_{12} = q_1 + q_2$. The function $\tilde{\Pi}_{(\rho)\mu\nu\lambda\sigma}$ is now only dependent upon two momenta since the limit $k \to 0$ for the external photon momentum has been carried out.

IV. RESULTS

With the approach to hadronic LBL scattering within the functional approach outlined, and our truncation scheme defined we proceed to combine our propagators, vertices, amplitudes, and form factors together and calculate the respective contributions to hadronic LBL scattering in the muon $g - 2$.

A. Pion-pole contribution to LBL

To demonstrate parity between our approach and others in the determination of hadronic LBL, we calculate the ladder-exchange diagram of Fig. 3 assuming pseudoscalar-pole dominance. Once more, we reiterate that on-mass-shell this is identical to the pseudoscalar exchange diagram portrayed in Fig. 2, whereas off-shell we make the common assumption that the meson-exchange picture provides a good approximation.

In order to determine the pseudoscalar exchange contribution we must numerically determine the dressed quark propagator, the quark-photon vertex, and the homogeneous Bethe-Salpeter amplitude for the pseudoscalar meson. Combining these together allows us to calculate from first principles the $\pi\gamma\gamma$ form factor. We wish to emphasize again that the resulting quark-photon vertex also contains timelike poles corresponding to vector meson exchange [49]. Thus the main ideas of VMD are naturally included here in the form factor due to the nonperturbative approach that we employ. We have checked that the total numerical error of our calculation is of the order of 1%. In a similar fashion we also evaluate the corresponding form factors for the η and η' mesons. We then use our results for the form factors to evaluate the pseudoscalar meson exchange contribution to LBL. For this, we use the off-shell prescription for the pseudoscalar Bethe-Salpeter amplitude proposed in Eq. (28) for the exchanged mesons. This prescription gives a reduction of the contribution that is similar to that found in other approaches.

The systematic error of our calculation of the pseudoscalar exchange diagrams can be attributed entirely to the validity of the rainbow-ladder approximation, by the MT model, Eq. (13), and the off-shell prescription for the mesons, Eq. (27). No other approximations have been used. While in the Goldstone-Boson sector the MT model works well, there is certainly a larger error in the flavor singlet sector. We therefore guesstimate a total systematic error: 10% for the pion contribution, and 20% for the η and η' contributions. With a numerical error of 2% we then obtain $a_\mu^{\mathrm{LBL};\pi^0} = (57.5 \pm 6.9) \times 10^{-11}$, $a_\mu^{\mathrm{LBL};\eta} = (13.6 \pm 3.0) \times 10^{-11}$, and $a_\mu^{\mathrm{LBL};\eta'} = (9.6 \pm 2.1) \times 10^{-11}$ leading to

$$a_\mu^{\mathrm{LBL;PS}} = (80.7 \pm 12.0) \times 10^{-11} \quad (33)$$

for the pseudoscalar meson-exchange contribution to LBL. As compared to our previous work [23], the values for $a_\mu^{\mathrm{LBL};\eta}$ and $a_\mu^{\mathrm{LBL};\eta'}$ are slightly reduced due to a more consistent off-shell prescription in these channels. Our result (33) is compatible with previous ones [5,6,17], which for the pion-pole contribution are displayed in Table II. This is not surprising, since the form factors themselves are compatible at a qualitative level, cf.

TABLE II. Results for the π^0-pole and quark-loop contribution (where appropriate) to hadronic light-by-light scattering, in different models are shown. For † the quark-loop correction is incorporated as a boundary condition on the pion-pole contribution, while for ‡ the quark-loop corrections are currently under investigation [58].

Group	Model	a_μ^{LBL} (π^0 pole)	a_μ^{LBL} (quark loop)
Bijnens, Prades, Pallante [16]	ENJL	59(11)	21(3)
Hayakawa, Kinoshita [10], HK and Sanda [8,9]	HLS	57(4)	9.7(11.1)
Knecht and Nyffeler [13]	LMD + V	58(10)	…
Melnikov and Vainshtein [14]	LMD + V	77(5)	†
Dorokhov and Broniowski [18]	NLχQM	65(2)	‡
Nyffeler [5]	LMD + V	72(12)	†
Our Result	DSE	58(10)	136(59)

Fig. 16, and all approaches make the assumption that pseudoscalar-pole dominance is valid far from the meson mass-shell.

B. Quark-loop contribution to LBL

Having convinced ourselves that the method works we now focus on the quark-loop contribution to LBL. Here we follow the strategy described around Eq. (6) where the Ward identity obeyed by the four-point function with respect to the external field is exploited to construct quantities that are explicitly finite. As for our numerical error we verified that we reproduce the well-known perturbative result for the corresponding electron loop with an accuracy of better than one per mille. In the quark loop we use the fully dressed quark propagators for the up, down, strange, and charm quarks, extracted from the DSE, Fig. 10. As already mentioned above, due to numerical complexity we are unfortunately not yet in a position where we can use the full, numerically determined quark-photon vertex used for the meson-exchange contributions in the previous section. Instead, we use three different approximations to the full vertex and compare the results. As explained in section III B due to the Ward-identity we are in possession of exact expressions for the non-transversal, Ball-Chiu (BC) part of the vertex, Eq. (19). We exploit this knowledge to compare results with (a) a bare vertex, (b) the first term of Eq. (19) (1BC)

$$\Gamma_\mu(p,q) = \frac{A(p^2)+A(q^2)}{2}\gamma_\mu, \tag{34}$$

where p, q are the quark and antiquark momenta, and (c) the full Ball-Chiu (BC) expression Eq. (19). A comparison between these three approximations may serve as a guide for the systematic error due to the relevance of vertex effects. We emphasize, however, that only our most elaborate approximation, (c), satisfies the constraints of gauge invariance. Previous approximations based on purely transverse parts of the vertex [16] do not satisfy this constraint. We believe that the ansatz (c) provides an excellent basis for the calculation of the quark-loop diagram, which can and should be expanded in future work to also include transverse parts of the vertex.

As a result of our calculation we find

$$\begin{aligned} a_\mu^{\text{LBL;quarkloop (bare vertex)}} &= (61 \pm 2)\times 10^{-11}, \\ a_\mu^{\text{LBL;quarkloop (1BC)}} &= (107 \pm 2)\times 10^{-11}, \\ a_\mu^{\text{LBL;quarkloop (BC)}} &= (176 \pm 4)\times 10^{-11}, \end{aligned} \tag{35}$$

for the quark-loop contribution. Clearly these are sizable contributions. Whereas the bare vertex result roughly agrees with the number 60×10^{-11} given in [14], the dressing effects of the vertex lead to a drastic increase. As compared to our result for the first part of the Ball-Chiu vertex [23] we again find a drastic increase from 107×10^{-11} to 176×10^{-11} when the other two terms of the full Ball-Chiu vertex are included. In this calculation we included effects from four quark flavours in the quark-loop. Their individual contributions are given by

$$\begin{aligned} a_\mu^{\text{LBL;quarkloop (BC);}u/d} &= (158 \pm 3)\times 10^{-11}, \\ a_\mu^{\text{LBL;quarkloop (BC);}s} &= (6 \pm 1)\times 10^{-11}, \\ a_\mu^{\text{LBL;quarkloop (BC);}c} &= (12 \pm 1)\times 10^{-11}. \end{aligned} \tag{36}$$

It is interesting to note that due to charge effects the heavy charm quark contributes more than the much lighter strange quark.

We have checked the model dependence of the above result by comparing with a similar calculation using a different model for the quark-gluon interaction [38]. The results are similar to the one in Eq. (35) within an error margin of five to 10%. Details will be given elsewhere. Because of these results we estimate an additional systematic error for our BC result of 15×10^{-11}, which has to be added to the 4×10^{-11} given in Eq. (35).

In general, these large dressing effects also make it very hard if not impossible to guess the effect of the total vertex dressing without an explicit calculation. Certainly, however, given these findings, all previous estimates for the systematic error in the quark-loop contributions seem to be an order of magnitude too small.

V. CONCLUSIONS

In this paper we have presented a new approach towards the anomalous magnetic moment of the muon. We have used a combination of Dyson-Schwinger and Bethe-Salpeter equations to evaluate the pseudoscalar meson-exchange contribution and the quark-loop contribution to LBL. Our only input is the Maris-Tandy model, a phenomenologically successful ansatz for the combined strength of the gluon propagator and the quark-gluon vertex. Our treatment of the meson-exchange contribution to LBL is different from earlier approaches in that we do not rely on an ansatz for the PS$\gamma\gamma$ form factor, but calculate this quantity starting from the basic equations of motion of QCD. Nevertheless, our result basically agrees with those from previous approaches. This result once more emphasizes that the meson-exchange contributions to LBL are largely controlled by analytic constraints from QCD at large and small Q^2.

As for the quark-loop contribution, analytic constraints have been used which arise from the requirement of gauge invariance: the quark-photon vertex appearing in this loop has to satisfy the vector Ward-Takahashy identity. In contrast to previous approaches, we have implemented this identity by using the Ball-Chiu ansatz for this vertex. We believe this is a systematic improvement. The consequences are drastic: we observe a dramatic increase for the quark-loop contribution to LBL. Our result of $(176 \pm 4)\times 10^{-11}$

is more than 3 times larger than the constituent quark result of Ref. [14].

When combining our two results, Eqs. (33) and (35), we arrive at a hadronic LBL contribution of

$$a_\mu^{\mathrm{LBL;PS+quarkloop}} = (257 \pm 31) \times 10^{-11}. \quad (37)$$

This value, however, does not yet account for transverse parts of the quark-photon vertex in the quark-loop contribution and for effects from the right-hand diagrams of Fig. 2 or Fig. 3. In general, it is difficult to gauge the effects of additional transverse vertex contributions in the quark-loop diagram. In Ref. [16] part of these effects have been taken into account by using an ansatz motivated by VMD ideas. They found a reduction due to these effects of roughly 40×10^{-11}. Since we agree with Ref. [16] on the size of the pion exchange contribution, where VMD works very well, it may be justified to use their result as a rough estimate for the size and also for the potential error in these effects. We therefore add a contribution[4] of $a_\mu^{\mathrm{LBL;quarkloop,transverse}} = (-40 \pm 40) \times 10^{-11}$ to arrive at $a_\mu^{\mathrm{LBL;quarkloop\ (BC+transverse)}} = (136 \pm 59) \times 10^{-11}$.

The additional contributions due to the right-hand diagrams of Fig. 2 or Fig. 3 are also difficult to judge. It may help, though, to observe that these involve an additional quark-loop. Typically such contributions are negative and of the order of 10 to 20 percent of the leading-N_c contributions [28,29]. Since on the other hand one also expects positive contributions of a similar size from nonpseudoscalar exchange diagrams [1] we choose to subsume all these contributions to another $a_\mu^{\mathrm{LBL;other}} = (0 \pm 20) \times 10^{-11}$, where the error is clearly subjective. This gives us the following total hadronic LBL contribution:

$$a_\mu^{\mathrm{LBL}} = (217 \pm 91) \times 10^{-11}, \quad (38)$$

in our approach. Note that the increase of the central value as compared to our previous result in Ref. [23] is due to a combination of taking the full BC-vertex instead of 1BC and in addition accounting for the transverse corrections in the quark-loop using the results of Ref. [16]. Taken at face value these numbers together with the other contributions quoted in [1] clearly reduce the discrepancy between theory and experiment. Combining our light-by-light scattering results with the other SM contributions gives

$$a_\mu^{\mathrm{theor.}} = 116\,591\,891.0(105.0) \times 10^{-11}. \quad (39)$$

To put this result in perspective we wish to recall the caveats that to our mind are tied to it. First, there is the contribution of transverse parts of the quark-photon vertex to the quark-loop diagram. Although the results of Ref. [16] may serve as an estimate, we definitely need to explicitly calculate these contributions in our approach. Second, there is the question whether the pseudoscalar meson-exchange diagram provides for a good approximation of the gluon exchange contribution discussed around Fig. 3. Also this assumption needs to be questioned by an explicit calculation. In this sense, our results certainly do not provide final answers but still have to be seen as a further step towards a fundamental determination of a_μ.

Finally, we point out that the current approach will also be checked by a calculation of the hadronic vacuum polarization contribution to a_μ. Preliminary results in this direction are encouraging.

ACKNOWLEDGMENTS

This work was supported by the Helmholtz-University Young Investigator Grant No. VH-NG-332 and by the Helmholtz International Center for FAIR within the LOEWE program of the State of Hesse.

[4]Note that cross terms between transverse and nontransverse contributions from the four vertices in the quark-box diagram could provide additional suppression. This is expressed in our error estimate.

[1] F. Jegerlehner and A. Nyffeler, Phys. Rep. **477**, 1 (2009).
[2] F. Jegerlehner, *The Anomalous Magnetic Moment of the Muon* (Springer, Berlin, 2008), p. 426.
[3] D. Stockinger, J. Phys. G **34**, R45 (2007).
[4] G. W. Bennett *et al.* (Muon $g-2$ Collaboration), Phys. Rev. D **73**, 072003 (2006).
[5] A. Nyffeler, Phys. Rev. D **79**, 073012 (2009).
[6] J. Prades, E. de Rafael, and A. Vainshtein, arXiv:0901.0306.
[7] J. Bijnens and J. Prades, Mod. Phys. Lett. A **22**, 767 (2007).
[8] M. Hayakawa, T. Kinoshita, and A. I. Sanda, Phys. Rev. Lett. **75**, 790 (1995).
[9] M. Hayakawa, T. Kinoshita, and A. I. Sanda, Phys. Rev. D **54**, 3137 (1996).
[10] M. Hayakawa and T. Kinoshita, Phys. Rev. D **57**, 465 (1998); **66**, 019902(E) (2002).
[11] G. Ecker, J. Gasser, H. Leutwyler, A. Pich, and E. de Rafael, Phys. Lett. B **223**, 425 (1989); G. Ecker, J. Gasser, A. Pich, and E. de Rafael, Nucl. Phys. **B321**, 311 (1989).
[12] E. de Rafael, Phys. Lett. B **322**, 239 (1994).
[13] M. Knecht and A. Nyffeler, Phys. Rev. D **65**, 073034 (2002).
[14] K. Melnikov and A. Vainshtein, Phys. Rev. D **70**, 113006 (2004).
[15] A. Nyffeler, Chinese Phys. C **34**, 705 (2010).

[16] J. Bijnens, E. Pallante, and J. Prades, Phys. Rev. Lett. **75**, 1447 (1995); **75**, 3781(E) (1995); Nucl. Phys. **B474**, 379 (1996).
[17] A. E. Dorokhov, Phys. Rev. D **70**, 094011 (2004).
[18] A. E. Dorokhov and W. Broniowski, Phys. Rev. D **78**, 073011 (2008).
[19] R. Alkofer and L. von Smekal, Phys. Rep. **353**, 281 (2001).
[20] P. Maris and C. D. Roberts, Int. J. Mod. Phys. E **12**, 297 (2003).
[21] C. S. Fischer, J. Phys. G **32**, R253 (2006).
[22] C. D. Roberts, Prog. Part. Nucl. Phys. **61**, 50 (2008).
[23] C. S. Fischer, T. Goecke, and R. Williams, Eur. Phys. J. A **47**, 28 (2011).
[24] J. Aldins, T. Kinoshita, S. J. Brodsky, and A. J. Dufner, Phys. Rev. Lett. **23**, 441 (1969).
[25] J. Aldins, T. Kinoshita, S. J. Brodsky, and A. J. Dufner, Phys. Rev. D **1**, 2378 (1970).
[26] P. Bicudo, S. Cotanch, F. J. Llanes-Estrada, P. Maris, E. Ribeiro, and A. Szczepaniak, Phys. Rev. D **65**, 076008 (2002).
[27] S. R. Cotanch and P. Maris, Phys. Rev. D **66**, 116010 (2002).
[28] C. S. Fischer, D. Nickel, and J. Wambach, Phys. Rev. D **76**, 094009 (2007).
[29] C. S. Fischer and R. Williams, Phys. Rev. D **78**, 074006 (2008); Phys. Rev. Lett. **103**, 122001 (2009); R. Williams, arXiv:0912.3494.
[30] T. Hahn, Comput. Phys. Commun. **168**, 78 (2005).
[31] T. Kinoshita, Phys. Rev. Lett. **61**, 2898 (1988).
[32] M. A. Samuel, Phys. Rev. D **45**, 2168 (1992).
[33] S. Laporta and E. Remiddi, Phys. Lett. B **301**, 440 (1993).
[34] J. A. M. Vermaseren, arXiv:math-ph/0010025.
[35] T. Reiter, Comput. Phys. Commun. **181**, 1301 (2010).
[36] P. Watson and W. Cassing, Few Body Syst. **35**, 99 (2004).
[37] F. D. R. Bonnet, P. O. Bowman, D. B. Leinweber, A. G. Williams, and J. M. Zanotti, Phys. Rev. D **64**, 034501 (2001).
[38] C. S. Fischer and R. Alkofer, Phys. Rev. D **67**, 094020 (2003).
[39] W. Kamleh, P. O. Bowman, D. B. Leinweber, A. G. Williams, and J. Zhang, Phys. Rev. D **76**, 094501 (2007).
[40] C. S. Fischer, A. Maas, and J. M. Pawlowski, Ann. Phys. (N.Y.) **324**, 2408 (2009).
[41] C. S. Fischer and J. A. Mueller, Phys. Rev. D **80**, 074029 (2009).
[42] J. I. Skullerud, P. O. Bowman, A. Kizilersu, D. B. Leinweber, and A. G. Williams, J. High Energy Phys. 04 (2003) 047.
[43] R. Alkofer, C. S. Fischer, F. J. Llanes-Estrada, and K. Schwenzer, Ann. Phys. (N.Y.) **324**, 106 (2009); R. Alkofer, C. S. Fischer, and F. J. Llanes-Estrada, Mod. Phys. Lett. A **23**, 1105 (2008).
[44] P. Maris and P. C. Tandy, Phys. Rev. C **60**, 055214 (1999).
[45] P. Maris, C. D. Roberts, and P. C. Tandy, Phys. Lett. B **420**, 267 (1998).
[46] P. Maris and C. D. Roberts, Phys. Rev. C **58**, 3659 (1998).
[47] J. S. Ball and T. W. Chiu, Phys. Rev. D **22**, 2542 (1980).
[48] P. Maris and P. C. Tandy, Phys. Rev. C **61**, 045202 (2000).
[49] P. Maris and P. C. Tandy, Nucl. Phys. **A663–664**, 401c (2000).
[50] P. Maris and P. C. Tandy, Phys. Rev. C **65**, 045211 (2002).
[51] M. S. Bhagwat and P. Maris, Phys. Rev. C **77**, 025203 (2008).
[52] T. Feldmann, P. Kroll, and B. Stech, Phys. Rev. D **58**, 114006 (1998); Phys. Lett. B **449**, 339 (1999).
[53] S. Adler, Phys. Rev. **177**, 2426 (1969); J. S. Bell and R. Jackiw, Nuovo Cimento A **60**, 47 (1969); J. Wess and B. Zumino, Phys. Lett. **37B**, 95 (1971); E. Witten, Nucl. Phys. **B223**, 422 (1983).
[54] L. von Smekal, A. Mecke, and R. Alkofer, AIP Conf. Proc., **412**, 746 (1997).
[55] M. S. Bhagwat, L. Chang, Y. -X. Liu, C. D. Roberts, and P. C. Tandy, Phys. Rev. C **76**, 045203 (2007).
[56] R. Alkofer, C. S. Fischer, and R. Williams, Eur. Phys. J. A **38**, 53 (2008).
[57] C. D. Roberts, Fiz. B **8**, 285 (1999).
[58] A. E. Dorokhov, A. E. Radzhabov, and A. S. Zhevlakov (unpublished).